J. Fluid Mech. (2007), *vol.* 575, *pp.* 57–82.
doi:10.1017/S0022112006004423 Printed in the United Kingdom

The flow structure of a bubble-driven liquid-metal jet in a horizontal magnetic field

C. ZHANG, S. ECKERT AND G. GERBETH

Forschungszentrum Dresden-Rossendorf e.V., PO Box 510119, 01314 Dresden, Germany
s.eckert@fzd.de

(Received 11 May 2006 and in revised form 28 September 2006)

Static magnetic fields are known to be suitable for damping mean flow and turbulent motion in an electrically conducting liquid. In this paper, an experimental study is presented considering the influence of a horizontal magnetic field on a bubble-driven flow of a liquid metal. The investigation is focused on the liquid circulation inside a liquid metal column driven by a central jet produced by gas injection. The fluid vessel has a circular cross-section and electrically insulating walls. Low gas flow rates were applied, resulting in a plume of separated bubbles rising inside a spot around the cylinder axis. This axisymmetric configuration is exposed to a horizontal magnetic field. We present detailed experimental data describing the spatial as well as the temporal structure of the velocity field. Measurements of the vertical and the radial velocity component, respectively, were performed using the ultrasound Doppler velocimetry (UDV), allowing for the first time a complete mapping of the liquid velocity distribution for a bubble-driven liquid metal flow. The magnetic field considerably modified the global and local properties of the flow field compared to an ordinary bubble plume. In the parameter range considered here we did not find a prior flow suppression, but, in fact, a restructuring of the convective motion. The original axisymmetric flow field became anisotropic with respect to the direction of the magnetic field lines. An upwards flow dominated in a plane parallel to the magnetic field, whereas the recirculating motion was enforced in the orthogonal plane. Contrary to usual expectations, the application of a moderate magnetic field ($100 < Ha < 400$, $1 \lesssim N \lesssim 10$) destabilizes the global flow and gives rise to transient, oscillating flow patterns with predominant frequencies.

1. Introduction

Owing to the Archimedes force, gas bubbles rise in a liquid metal bath and accelerate the surrounding fluid. In this manner a global motion is created in an initially quiescent fluid. Such bubble plumes have found wide applications in both metallurgical and chemical engineering processes. In the case of metallurgical refining or smelting operations, gas is injected to enhance mixing in the melt and to support chemical reactions. The structure and distribution of the gas phase and the flow field induced in the liquid phase are the key properties of interest. Magnetic fields can be used in practice to control, to some extent, both the flow pattern and the phase distribution and, hence, the efficiency of the considered metallurgical process. Suitable combinations of external magnetic fields and gas bubble injections allow adjustment to a favourable flow field with respect to an optimization of the final product quality.

The fluid dynamics of dispersed, compressible flows in general, and the impact of an external magnetic field in particular, are known to be extremely complex. Different

length and time scales coexist even in a rather generic flow configuration such as a bubble plume. Flow phenomena occurring in a gas-agitated bath can be classified according to their location in different regions with inevitable interaction: the near-nozzle region, the gas-liquid plume, the surrounding liquid and the surface region. A multitude of experimental investigations concerning the flow in bubble plumes has already been published, by Milgram (1983), Leitch & Baines (1989) and Iguchi *et al.* (1992, 1994), amongst others done either with water or with appropriate metallic melts. A comprehensive review on the dynamics in bubble columns can be found in Mudde (2005).

The influence of a horizontal DC magnetic field on the vertical jet inside a liquid metal column owing to gas-lift pumping is investigated in this paper. The rising bubbles are employed here as a special option to force a circulation inside the liquid metal. Regardless of the two-phase flow being confined to the region around the axis of the fluid vessel, the ascending flow appears to be closely related to the case of a buoyant jet considered by Davidson (1995). In this sense, specific features of a bubble plume, such as the bubble acceleration in the region near the gas injecting nozzle, the local flow around the bubbles, or the interaction between neighbouring bubbles, are not the focus of our study. Experimental results with respect to the effect of an external magnetic field on the local flow around a single bubble have already been published by Zhang, Eckert, & Gerbeth (2005), and will not be considered here.

A predominantly damping effect on three-dimensional flow structures is expected if an electrically conducting liquid is subjected to a DC magnetic field. Engineering approaches for electromagnetic flow control employ the concept of electromagnetic braking, for instance in the continuous casting of liquid metals. The crucial non-dimensional parameters to describe the ratio of the Lorenz force $\boldsymbol{F} = \boldsymbol{j} \times \boldsymbol{B}$, that arises from the interaction between the electric current $\boldsymbol{j}$ induced in the liquid and the applied field $\boldsymbol{B}$, to the viscous or inertial forces are the Hartmann number Ha and the magnetic interaction parameter N, respectively:

$$Ha = BR\sqrt{\frac{\sigma}{\rho\nu}}, \tag{1.1}$$

$$N = \frac{\sigma RB^2}{\rho U_L}, \tag{1.2}$$

where ρ, ν and σ stand for the liquid properties density, kinematic viscosity and electrical conductivity, respectively. R is the typical length scale, namely the radius of the fluid vessel. The time-averaged liquid velocity inside the bubble plume U_L is used here as a typical velocity scale. The measurements to be presented in this paper were performed in a parameter range ($Ha \gg 1$, $N > 1$) where a strong influence of the magnetic field on the flow structure can be expected. It is known that the anisotropy of the electromagnetic dissipation promotes a reorganization of the velocity field towards a two-dimensional state. Sommeria & Moreau (1982) have shown the tendency of vorticity to align with the magnetic field lines. A spreading of momentum along the magnetic field lines is a well-known phenomenon in the context of MHD turbulence, leading to a preferential formation of the flow structures parallel to the magnetic field (Davidson 1995). A purely two-dimensional state can hardly be achieved if the fluid is confined by walls being non-parallel with respect to the magnetic field lines. However, a cylinder with a circular cross-section was chosen as the fluid vessel in our experiment, because such a geometry is typical for applications in metallurgy and chemical engineering.

The investigations presented here did not include the effect of variations of the wall conductivity on the flow pattern. The measurements were restricted to the flow in an

electrically insulating container, because this situation is equivalent to the majority of cases in industrial operations. For instance, fluid containers made from ceramic materials are used to withstand the metallic melts at high temperatures.

Numerous studies have been published concerning the impact of a DC magnetic field on natural convection in liquid metals. Papailiou & Lykoudis (1968) investigated the effect of a horizontal magnetic field on a natural convection arising from a vertical heated plate in mercury. The magnetic field was aligned normally to the heated plate. For this configuration the heat transfer rate by convection was observed to decrease continuously with increasing magnetic field strength. Analogous results were reported by Tokuhiro & Lykoudis (1994) considering the same experimental setup with an additional gas injection at the bottom end of the heated plate. Other studies of natural convection in liquid metals showed that an imposed DC magnetic field did not always decrease the transport of heat. Tagawa & Ozoe (1997) investigated the natural convection in a cubical enclosure numerically, arising from heating one vertical wall and cooling the opposite one. A horizontal magnetic field B_0 has been applied parallel to the tempered walls. The results showed, for a wide range of Rayleigh numbers, that a weak magnetic field slightly enhances the convective heat transfer, manifested by an increasing Nusselt number, while a further increase of B_0 finally decreases the convective heat transfer. The numerical predictions were verified in experiments where an averaged Nusselt number was determined as a function of B_0. Similar results were found in experimental and numerical studies done by Burr *et al.* (2003), Tagawa, Authie & Moreau (2002) and Authie, Tagawa & Moreau (2003) considering buoyant flows in long vertical enclosures in a horizontal magnetic field applied perpendicularly to the horizontal temperature gradient. Compared to the case without a magnetic field the convective heat transport was observed by Burr *et al.* (2003) to be significantly enhanced for Hartmann numbers $Ha < 400$. The authors suggest that the damping effect of the Joule dissipation on the convective motion is counterbalanced by an ordering effect of the magnetic field which may dominate and improve the heat transfer rates. Measured spectra of temperature fluctuations indicate the formation of larger-scale vortices being more effective in convective heat transport as compared to the ordinary flow without magnetic field. Authie *et al.* (2003) found the magnetic damping to be much less in the case when the magnetic field is perpendicular to the temperature gradient, as compared to a parallel alignment of magnetic field and temperature gradient. For the perpendicular case the experimental data exhibit maximum Nusselt numbers at Hartmann numbers $Ha = 200 \ldots 300$. Experimental and analytical results from Rayleigh–Bénard convection, under the influence of a horizontal magnetic field, were reported by Burr & Müller (2002). Further, for this configuration the authors observed regions with enhanced heat transfer compared to the ordinary flow. Local isotropy coefficients of the local temperature gradient show that the increase of the heat transfer is associated with an increasingly non-isotropic state of convection rolls becoming aligned with the magnetic field lines.

This paper is organized as follows. Section 2 contains the description of the experimental setup. The results of the velocity measurements will be presented in § 3, followed by a discussion in § 4.

2. Experimental setup

The experimental setup is shown in figure 1. The experiments were conducted under isothermal conditions at room temperature. The eutectic alloy $Ga^{68}In^{20}Sn^{12}$ (melting point 10 °C) was retained in a cylindrical container made from Plexiglas having an inner diameter $D = 2R$ of 90 mm. The height H of the liquid metal column was

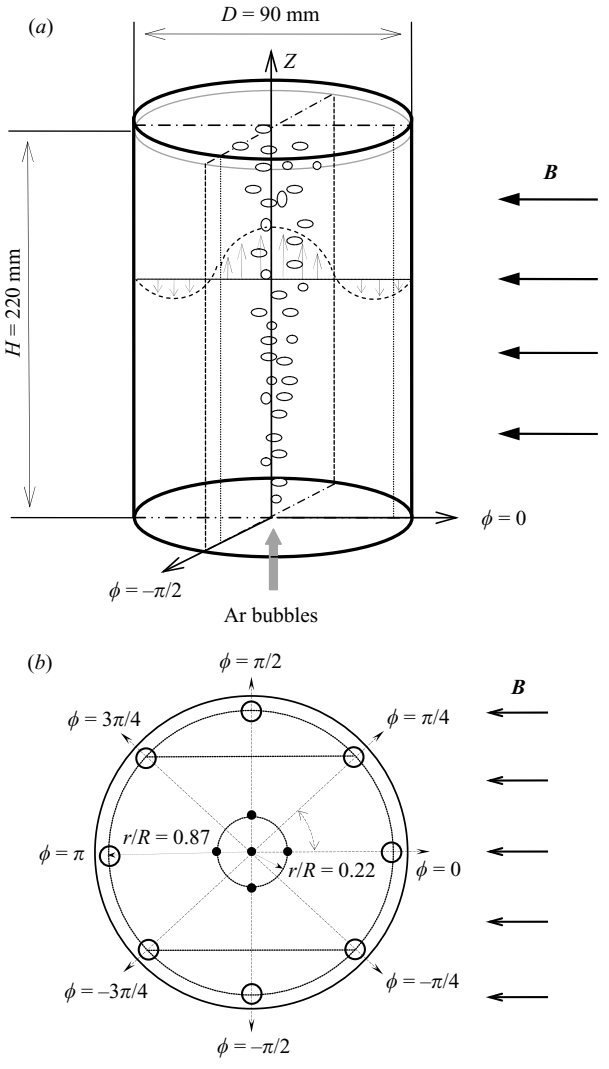

FIGURE 1. Sketch of the experimental setup: (*a*) schematic view of the bubble column configuration; (*b*) container cross-section with indicated measuring positions used for the conductance probes (marked by ●) and UDV sensors (marked by ○).

chosen to be 220 mm leading to an aspect ratio $A = H/2R = 2.44$. Argon gas was injected through a single-hole nozzle with an inner diameter d_N of 1 mm located at the container bottom in the centre of the circular cross-section. The gas flow rate Q_g was adjusted using a mass flow controller (MKS 1359C, MKS Instruments). Experiments were carried out in a range of low gas flow rates ($Q_g = 0.33$–$6.67\,\mathrm{cm^3\,s^{-1}}$) to ensure the formation of a dispersed bubbly flow regime. A Helmholtz configuration of a pair of water-cooled copper coils was used to generate a transverse DC magnetic field. This magnetic system delivers a homogenous magnetic field covering the full volume of the liquid metal. The magnetic field direction was selected along the y-coordinate. The gas bubbles rise almost parallel to the cylinder axis, being identical to the z-axis of our coordinate system. In our experiments magnetic fields were applied up to a

maximum strength of 0.28 T corresponding to a maximum Hartmann number of $Ha = 484$.

The DOP2000 velocimeter (model 2125, Signal Processing SA) alternatively equipped with standard 4 MHz (TR0405LS) or 8 MHZ (TR0805LS) transducers, respectively, was used to carry out the velocity measurements. The measuring principle of the Ultrasound Doppler Velocimetry (UDV) is based on the pulsed echo technique and described in detail by Takeda (1991). The UDV technique provides an instantaneous profile of the velocity measured along the ultrasonic beam. The measuring volume can be considered as a series of disks lined up concentrically along the measuring line. The size of the individual disks depends on several factors such as the sound velocity of the liquid, the frequency and the diameter of the piezoelectric element and the number of cycles forming one burst. Because of the divergence of the ultrasonic beam the size of the measuring volume in lateral direction increases with the distance from the transducer. Employing the standard 8 MHz transducer, we achieved a spatial resolution of about 0.69 mm in axial and 7.1 mm in lateral direction in a distance of 100 mm ahead of the transducer, respectively. The velocity profiles were recorded with a sampling rate of 27.5 Hz given by a pulse repetition frequency of 2370 Hz for the consecutive bursts and an averaging procedure including 60 bursts per profile. A velocity resolution of about $1.5\,\mathrm{mm\,s^{-1}}$ was achieved. The ultrasonic transducer was installed outside the cylinder both at the bottom wall and the cylinder sidewall for the measurement of the vertical and the radial velocity component, respectively. A reproducible positioning of the ultrasonic sensors at the cylinder walls was achieved by means of a traversing system. The feasibility of velocity profile measurements by UDV in various liquid metals has already been demonstrated by Takeda & Kikura (2002), Brito *et al.* (2001) and, especially under the conditions of an external magnetic field, Eckert & Gerbeth (2002). A more detailed assessment of the specific problems arising in the context of UDV measurements in liquid metal experiments, such as the acoustic coupling, resonance effects connected with the transmission through material interfaces or the allocation of suitable tracer particles, can be found in Cramer, Zhang & Eckert (2004). Successful applications of the UDV technique in two-phase flows have also been reported by Wang *et al.* (2003) and Zhang, Eckert & Gerbeth (2004) showing the capability to measure simultaneously the bubble and the liquid velocity. In this paper, all results concerning the velocity field represent the liquid phase velocity. To extract the liquid velocity from the measuring signal the probability density function of the measured velocity data was examined. Usually, two peaks corresponding to the velocity of the liquid and gaseous phase, respectively, can be detected there. Multiple reflections of the ultrasonic beam between the gas bubbles occurring at higher gas flow rates may cause a blurring of these peaks, and hence, complicate a precise discrimination between both phase velocities. An iterative threshold method (Zhang *et al.* 2004) was applied to obtain accurate velocity profiles by identifying and excluding artefacts in the signal. The signal quality deteriorates with increasing gas flow rate. Accompanying LDV measurements in a transparent liquid showed gradual failures of this method at void fractions of 10 % and more. The low gas flow rates in the present study guarantee measuring the liquid flow with a reasonable accuracy.

Radial profiles of the void fraction, or rather the local bubble number, in the container cross-section were measured by single-wire conductance probes. This kind of sensor represents a standard technique in two-phase flows (Serizawa, Kataoka & Michiyshi 1975) and has already been applied for the application in liquid metals flows (Eckert, Gerbeth & Lielausis (2000*a*)). Two quantities are recorded during the

measurements, the number of bubbles occurring at the sensor position and their particular contact times with the sensor tip. The ratio of the gas contact time arising from an ensemble of bubbles and the corresponding entire measuring time is related to the local void fraction. In our experiments carried out at relatively low gas flow rates, the contact time of the particular bubbles does not vary noticeably for different sensor positions or magnetic field intensities. Thus, measuring results presented in terms of the void fraction and the bubble number, respectively, provide equivalent information.

3. Experimental results

3.1. *Impact of the magnetic field on the bubble plume*

Because gas bubbles can be considered as electrically non-conducting inclusions inside the liquid metal, they do not experience a direct force action arising from the application of a DC magnetic field. However, a rising bubble provokes a flow in the circumfluent liquid phase which is strongly affected by the electromagnetic force. The magnetically induced modifications of the liquid flow field have consequences on the bubble motion. An experimental study by Eckert *et al.* (2000*a*) was devoted to the lateral dispersion of a bubble swarm in a turbulent liquid metal channel flow in an imposed transverse magnetic field. The gas phase was injected by a single orifice positioned in the centre of the cross-section. An anisotropic distribution of the void fraction was found arising from a drastic decrease of the bubble dispersion coefficient along the magnetic field lines, whereas a moderate damping of the mass transfer properties was observed in the direction perpendicular to the field. The local mass transfer is governed by the anisotropic character of turbulent MHD flows dominated by the existence of quasi-two-dimensional vortices at $Ha \gg 1$.

In the present experiment a first qualitative assessment of the bubble plume behaviour could be achieved by a visual monitoring of the free surface of the liquid metal column. In the conventional case without magnetic field gas bubbles emerge isotropically all over the cross-section, whereas the maximum bubble number was observed at the centre. The application of the magnetic field causes a concentration of the bubbles inside a smaller bounded spot. The position of this spot is not fixed, but shows a low-frequency oscillation along the diameter of the liquid metal column perpendicular to the direction of the magnetic field.

Radial distributions of the void fraction measured at a height of 200 mm ($Z/H = 0.9$) are presented in figure 2. The application of the magnetic field leads to a concentration of the gas bubbles in the central region around the axis of the fluid vessel. The focusing of the gas phase advances non-isotropically with increasing magnetic field strength and is more pronounced along the direction parallel to the magnetic field ($\phi = 0$). This finding conforms in principle to the results from the MHD channel flow (Eckert *et al.* 2000*a*). In addition, three local conductance probes were utilized to count simultaneously the number of bubbles occurring at the cylinder axis ($r/R = 0$) and at four positions at $r/R = 0.22$ in the planes perpendicular and parallel to the magnetic field, respectively. Time series of the recorded bubble number were obtained consisting of consecutively measured data points each with a time interval of 5 s. The curves in figure 3 result from a spline interpolation. According to our visual observation at the free surface, the data displayed in figure 3 also reflect the periodically lateral motion of the bubble plume, which corresponds to considerable oscillations of the locally detected bubble number in the plane perpendicular to the magnetic field. The coincidence of maximum and minimum of

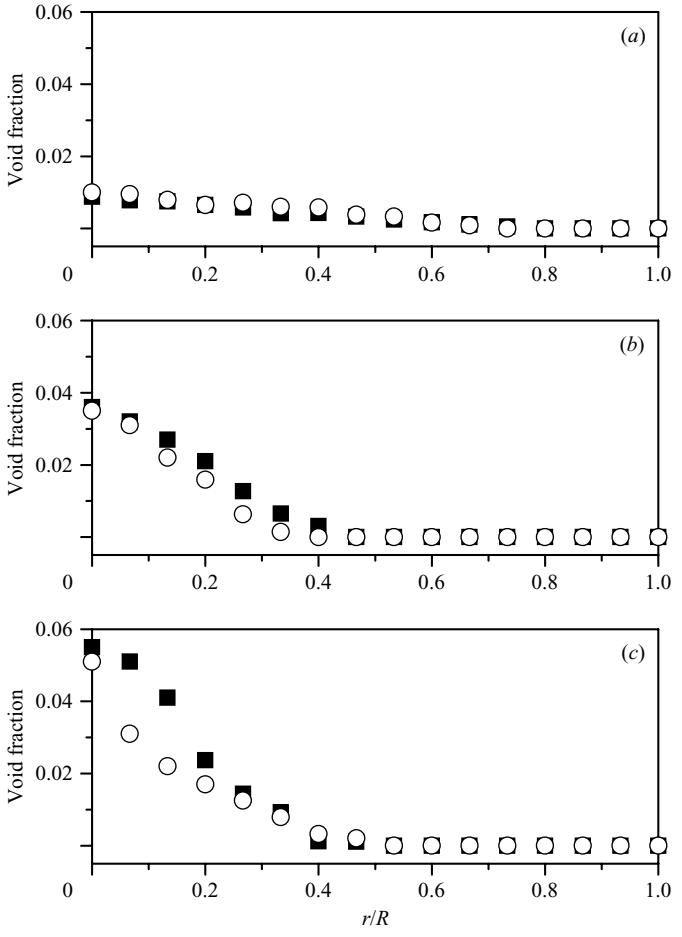

FIGURE 2. Time-averaged radial distributions of the local void fraction measured by a conductance probe at various Hartmann numbers: (*a*) $Ha = 0$; (*b*) $Ha = 271$; (*c*) $Ha = 484$. (■ denotes the distribution along the radius at $\phi = \pi/2$; ○ denotes the distribution along the radius at $\phi = 0$.) The data were acquired at the height of $Z/H = 0.9$ applying a gas flow rate of $Q_g = 3.67\,\mathrm{cm^3\,s^{-1}}$.

the curves measured at $\phi = \pm\pi/2$ indicates an alternate incidence of the focal point of the bubble concentration on either side of the cylinder axis. Long-term observations revealed a mean periodicity of about 15 s. It is worth noting that an increase of the Hartmann number (figure 3(*c*)) does not result in a reduction of the oscillation amplitude at $\phi = \pm\pi/2$.

3.2. *Time-averaged, spatial structure of the liquid flow*

Since the effect of a DC magnetic field on a liquid metal flow is known to be anisotropic with respect to the direction of the magnetic field, the velocity measurements were performed in two orthogonal midplanes parallel and perpendicular to the field lines, later referred to as parallel ($\phi = 0$) and perpendicular plane ($\phi = \pi/2$), respectively (see also figure 1). For reasons of presumed axial symmetry regarding the flow structure within each plane, the measurements were restricted to a half-plane. To obtain a time-averaged two-dimensional map of the flow both the vertical and the

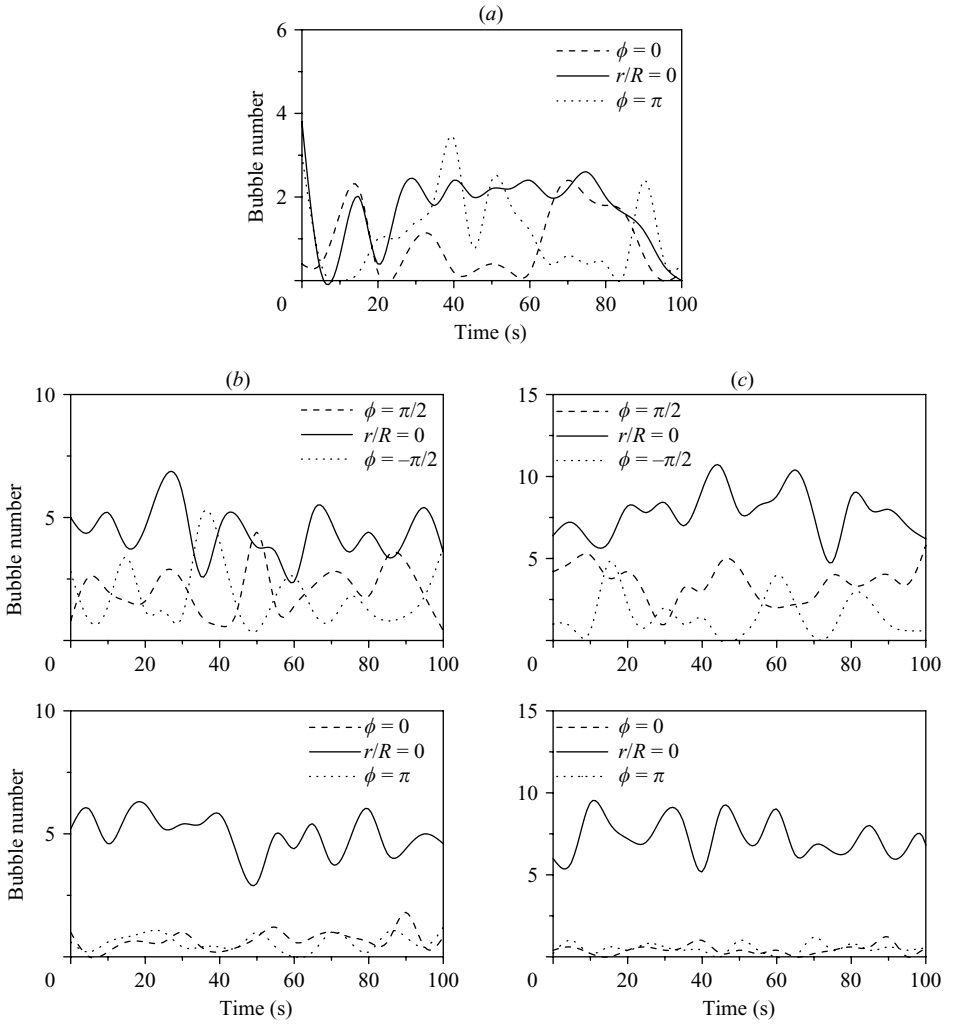

FIGURE 3. Time series of the locally counted bubble number (s^{-1}) at various Hartmann numbers simultaneously measured by 3 conductance probes: (*a*) $Ha = 0$; (*b*) $Ha = 271$; (*c*) $Ha = 484$. The data were acquired at the height of $Z/H = 0.9$ applying a gas flow rate of $Q_g = 3.67\,\mathrm{cm^3\,s^{-1}}$.

radial velocity components were measured. The ultrasonic sensors were moved with steps of 5 mm along the vertical wall and 3 mm at the bottom of the fluid container, respectively. The velocity profiles at each spatial position result from an averaging process over a measuring time of about 3 minutes. This period was found to be long enough to yield reliable, statistically trustworthy results. In all figures below an upward flow is represented by positive velocity values.

Figure 4 displays time-averaged flow patterns obtained at a relatively low gas flow rate of $0.33\,\mathrm{cm^3\,s^{-1}}$. The velocity field in each plane is visualized by the velocity vectors. The flow being typical for an ordinary bubble plume is shown in figures 4(*a*) and 4(*b*). Similar flow structures can be detected in both orthogonal planes. In the central region of the fluid container the liquid metal is driven upwards by the rising gas bubbles. The corresponding downward motion appears in the regions close to the

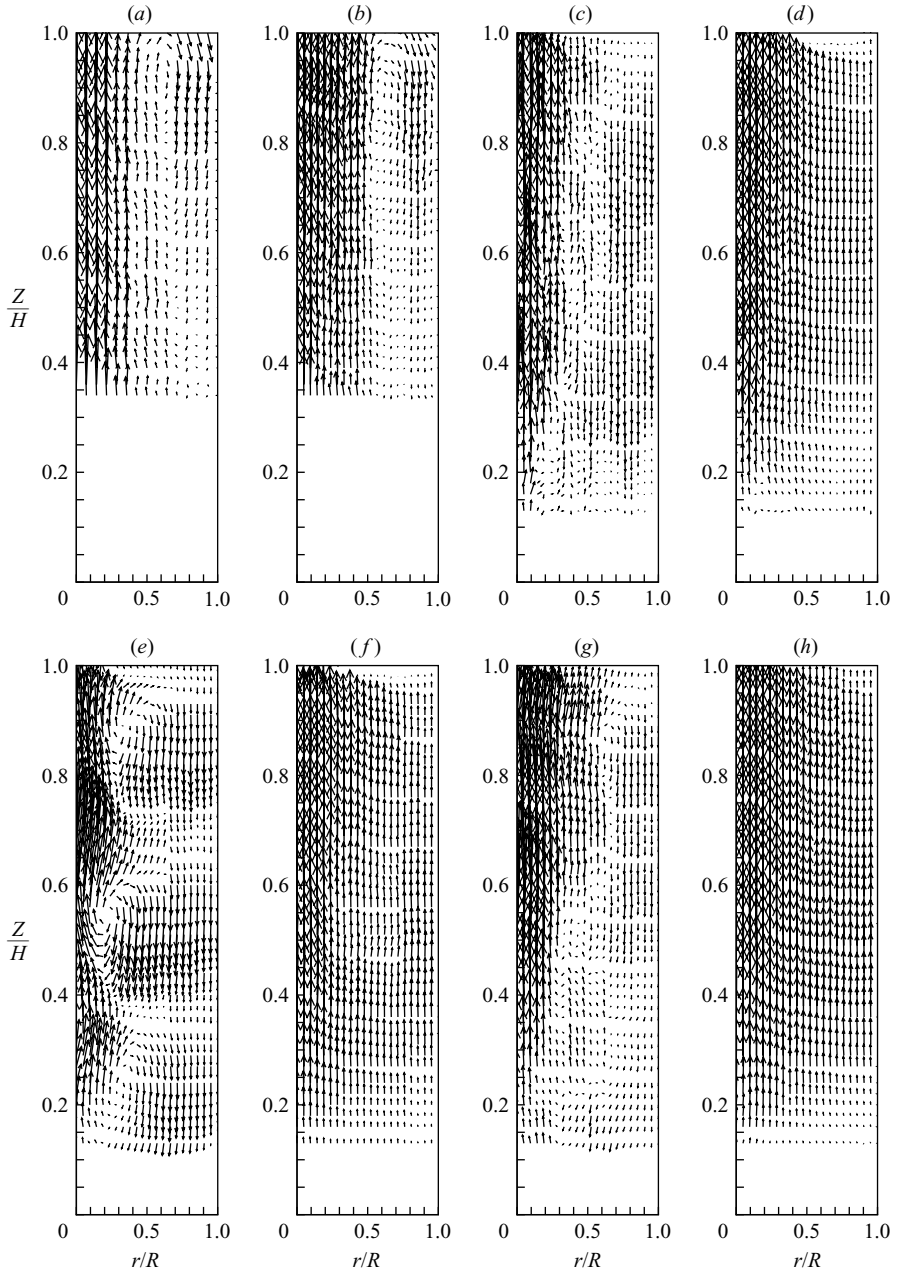

FIGURE 4. Vector plots of the liquid velocity structure at various Hartmann numbers: (*a*), (*b*) $Ha = 0$; (*c*), (*d*) $Ha = 162$; (*e*), (*f*) $Ha = 271$; (*g*), (*h*) $Ha = 484$. Figures (*a*), (*c*), (*e*), (*g*) display the flow in the perpendicular plane; and (*b*), (*d*), (*f*), (*h*) display the flow in the parallel plane ($Q_g = 0.33\,\mathrm{cm^3\,s^{-1}}$).

side walls. The application of a magnetic field changes the velocity field considerably, which becomes anisotropic as illustrated in figures 4(*c*)–4(*h*). Different flow patterns can be observed in both the parallel and perpendicular plane. The downward motion in the parallel plane is obstructed by the magnetic field, whereas an intensification of

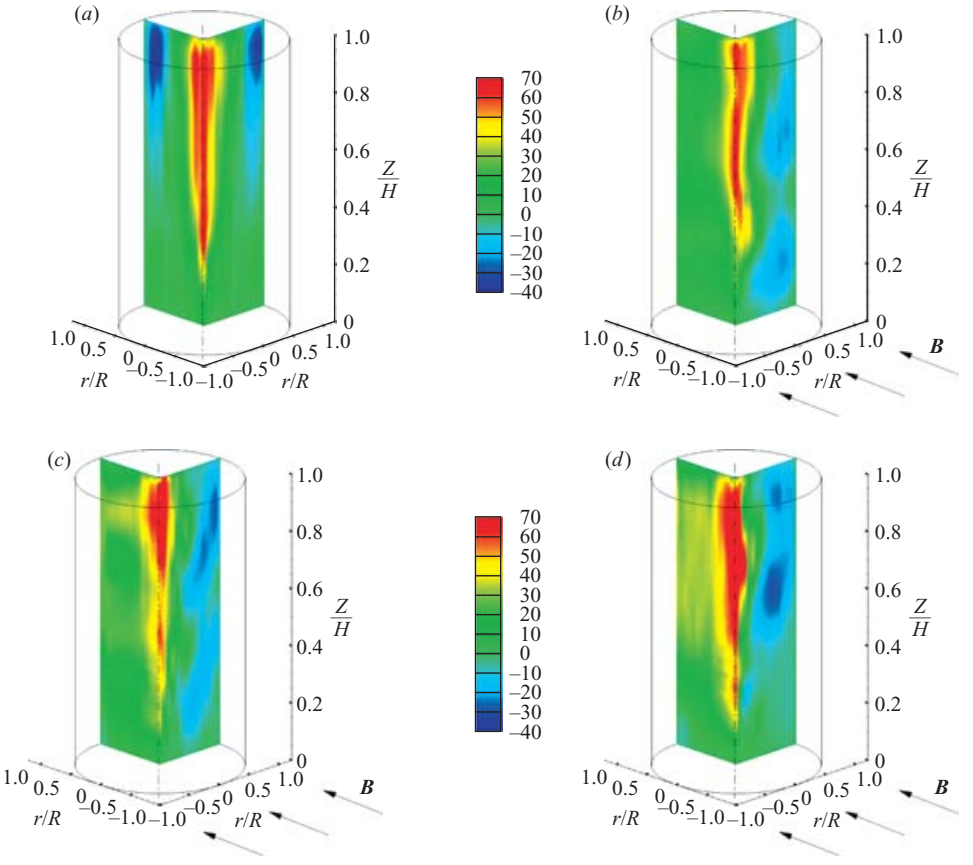

FIGURE 5. Contour plots of the vertical velocity component at various Hartmann numbers: (*a*) $Ha = 0$; (*b*) $Ha = 162$; (*c*) $Ha = 271$; (*d*)$Ha = 484$ ($Q_g = 0.83\,\mathrm{cm^3\,s^{-1}}$). The colour bar denotes the velocity in $\mathrm{mm\,s^{-1}}$.

the circulation can be observed in the perpendicular plane. A distinct vortical flow structure appears at a Hartmann number of 271 (see figure 4*e*), which is damped in turn with further increase of the magnetic field strength (figure 4*g*). Equivalent velocity measurements performed at higher gas flow rates revealed qualitatively analogue flow patterns.

Two-dimensional plots of the vertical velocity obtained at a gas flow rate of $0.83\,\mathrm{cm^3\,s^{-1}}$ are shown in figure 5. For reasons of a perspicuous presentation the velocity vectors are not drawn here. Corresponding profiles of the vertical velocity along the radius r/R and the height Z/H are presented in figures 6 and 7, respectively. The flow pattern of the ordinary bubble plume appears as almost axisymmetric. The maximum of the upward flow and the recirculation can be observed directly beneath the free surface. Substantial modifications of the flow structure are noticed in the case of an applied magnetic field. Considering the flow in the perpendicular plane, the recirculation is intensified in the lower region of the vessel. Moreover, the zones of recirculation are extended closer to the axis of the fluid container. On the other hand, the fluid is set in an upwards motion in the overall plane parallel to the magnetic field. A similar phenomenon has already been discussed by Davidson (1995,

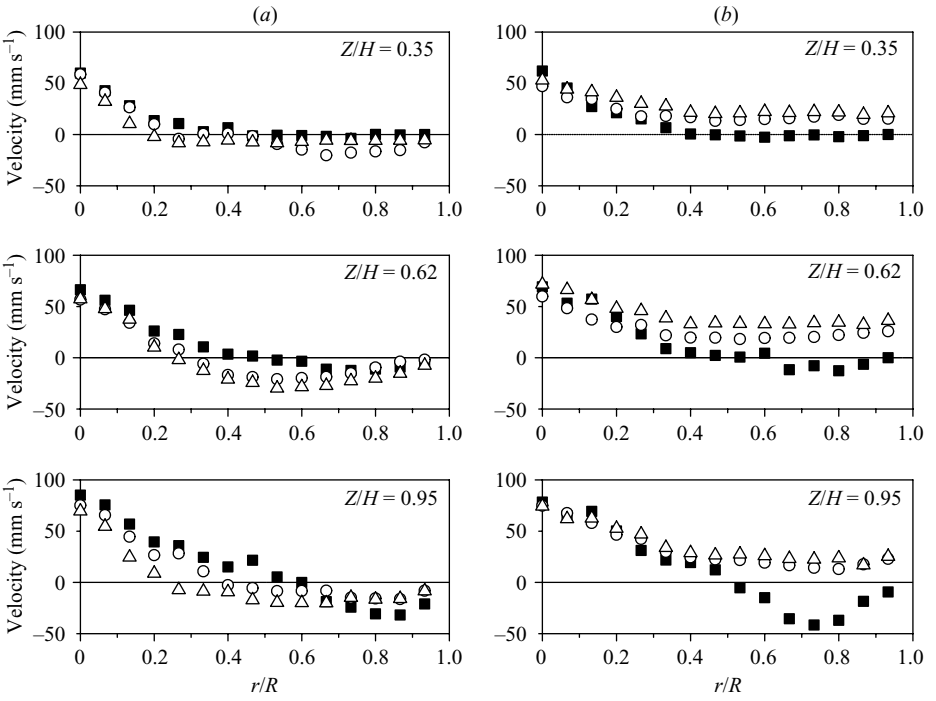

FIGURE 6. Radial distributions of the vertical velocity component at different heights and various Hartmann numbers: (*a*) in the plane perpendicular to $\boldsymbol{B}$; (*b*) in the plane parallel to $\boldsymbol{B}$. (■ denotes $Ha = 0$; ○ denotes $Ha = 271$; △ denotes $Ha = 484$; $Q_g = 0.83\,\mathrm{cm^3\,s^{-1}}$).

2001). Examples of generic flows in an imposed external magnetic field were shown to evolve in such a manner that their Joule dissipation will be minimized, which is achieved by a propagation of linear or angular momentum parallel to the magnetic field. In case of a circular jet the Joule dissipation is reduced if the cross-section of the jet has been stretched along the field lines. This mechanism is responsible for the reorganization of the velocity field observed in our experiment. The equalization of the radial velocity distribution towards a uniform ascending flow in the midplane along the magnetic field lines becomes apparent in figure 6, where selective radial profiles of the vertical velocity obtained at different heights are shown. At the same time the reverse, descending flow is promoted in the perpendicular midplane. Finally, distributions of the vertical velocity along the z-direction are displayed in figure 7, recorded at radial positions of $r/R = 0.87$ for both parallel and perpendicular midplanes. The anisotropy of the flow field in the MHD case is again confirmed. Periodic variations of the velocity profiles, as shown in figure 7(*a*), correspond to the vortical structure of the flow field, as already disclosed in figure 5. Considering the parallel plane, the magnetic field application leads to the definite reversal of the mean velocity profiles. The curves for an ordinary bubble plume show a zero-crossing, indicating the existence of small vortices in the lower corners counter-rotating with respect to the global recirculation. Owing to the magnetic field application these zero points disappeared (figure 7*a*) or were shifted downwards (figure 7*b*).

Figure 8 presents the time-averaged velocity and the RMS values as a function of the Hartmann number for gas flow rates of $0.83\,\mathrm{cm^3\,s^{-1}}$ and $3.67\,\mathrm{cm^3\,s^{-1}}$, respectively. The values have been deduced from velocity time series at the position $r/R = 0.87$ and

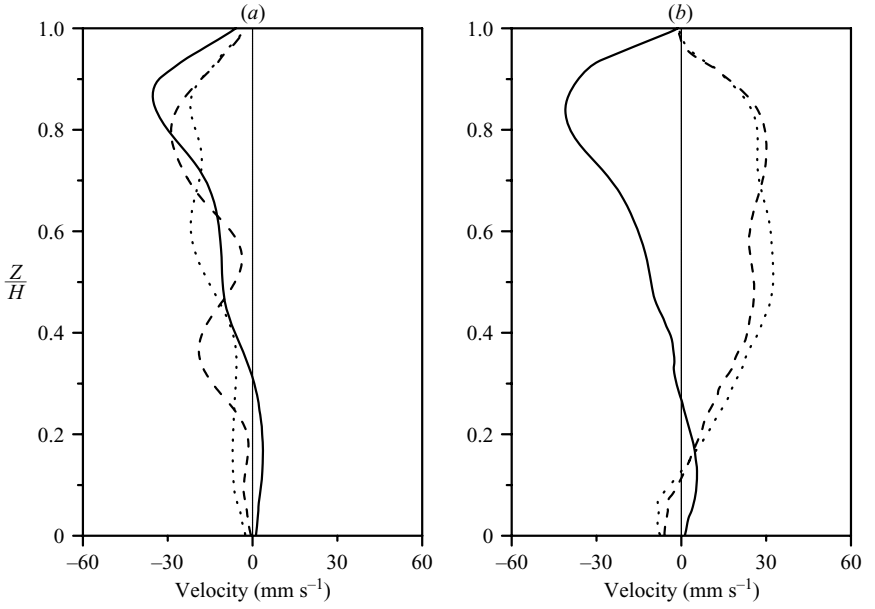

FIGURE 7. Vertical distributions of the vertical velocity component at various Hartmann numbers: (*a*) in the plane perpendicular to $\boldsymbol{B}$; (*b*) in the plane parallel to $\boldsymbol{B}$; ——, $Ha = 0$; – – –, $Ha = 271$; · · · · · ·, $Ha = 484$. The data were acquired at a radial position of $r/R = 0.87$ applying a gas flow rate of $Q_g = 0.83\,\mathrm{cm^3\,s^{-1}}$.

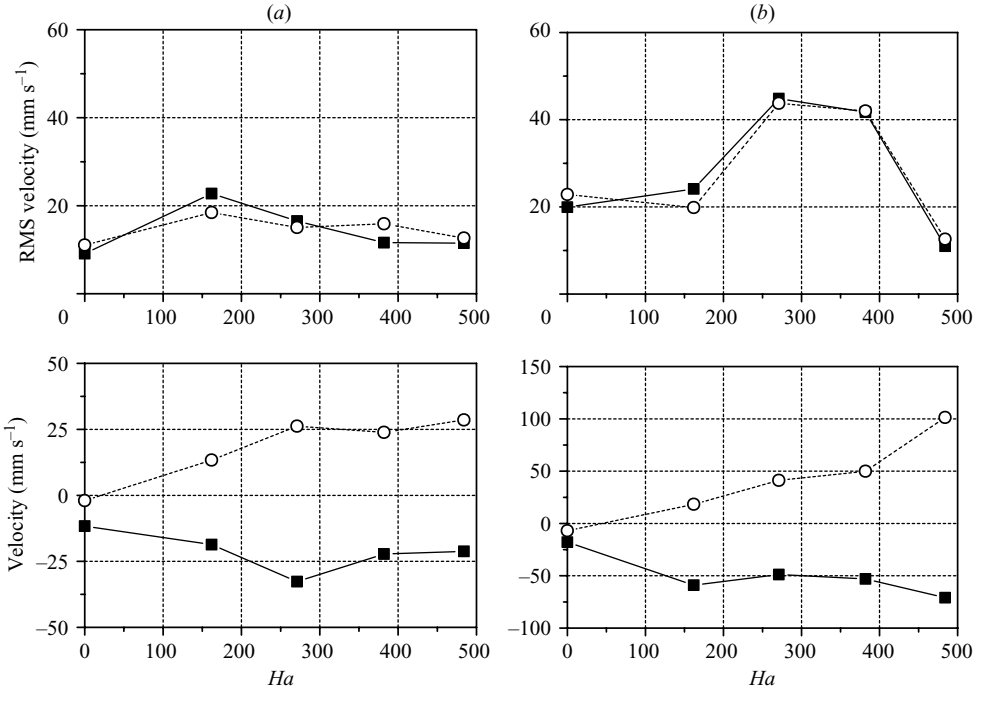

FIGURE 8. RMS values and time-averaged velocities calculated for different Hartmann numbers and two gas flow rates: (*a*) $Q_g = 0.83\,\mathrm{cm^3\,s^{-1}}$; (*b*) $Q_g = 3.67\,\mathrm{cm^3\,s^{-1}}$. (—■— denotes the flow in the perpendicular plane; ···○··· denotes the flow in the parallel plane.) The data were acquired at the position $r/R = 0.87$ and $Z/H = 0.5$.

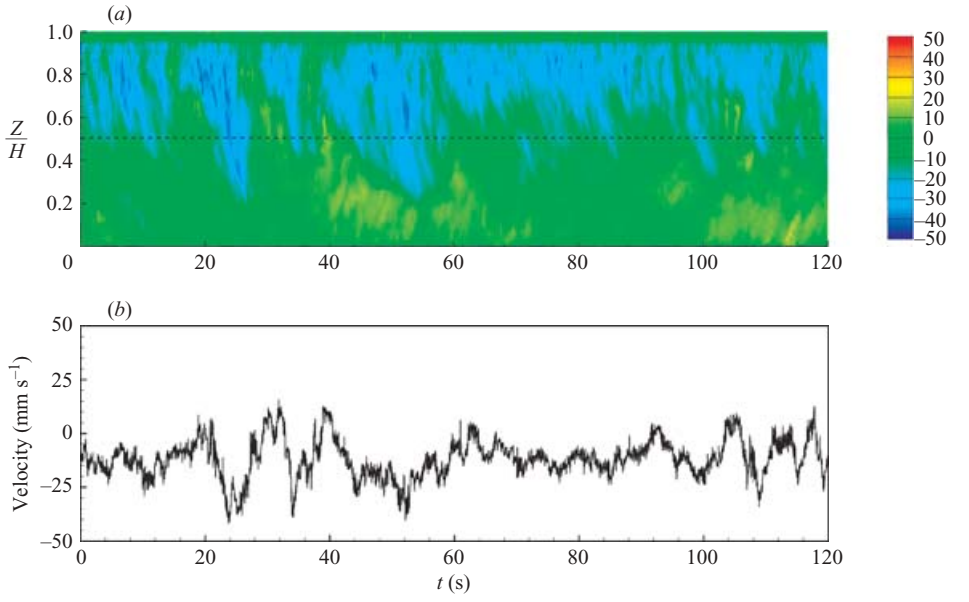

FIGURE 9. Vertical velocity measured along a vertical line at $r/R = 0.87$, $\phi = 0$, $Q_g = 0.83\,\mathrm{cm^3\,s^{-1}}$ and $Ha = 0$: (*a*) the spatiotemporal distribution; (*b*) selected time series at the position $Z/H = 0.5$. The colour bar denotes the velocity in $\mathrm{mm\,s^{-1}}$.

$Z/H = 0.5$. As shown in figure 8, the absolute value of the time-averaged velocity in both the parallel and perpendicular plane grows almost continuously with increasing Hartmann number. Furthermore, a considerable enhancement of the measured velocity variances (RMS) indicate that the magnetic field application at moderate field strengths ($Ha = 162$ at $Q_g = 0.83\,\mathrm{cm^3\,s^{-1}}$ or $Ha = 271$ at $Q_g = 3.67\,\mathrm{cm^3\,s^{-1}}$) gives rise to an increase of velocity fluctuations connected with the occurrence of large coherent flow structures. A further increase of the Hartmann number results in a damping of the oscillating flow structures accompanied by a significant decrease of the RMS value. This tendency can also be supported qualitatively by the analysis of the transient flow to be presented in the next section. However, the decrease of the RMS value is accompanied by a particular increment concerning the magnitude of the mean velocity. The kinetic energy contained in the slowly oscillating flow structures is probably not entirely dissipated by the Joule effect, but rather transferred towards the mean flow to some extent.

3.3. *Transient behaviour of the liquid flow*

The results on the spatial flow structure presented in the previous section revealed that the application of a transverse magnetic field gives rise to the occurrence of large coherent structures in the flow field. In this section the transient behaviour of these structures will be considered. For that reason time series of the vertical velocity profiles were recorded along a vertical line in both orthogonal planes as well as at measuring points in between. An overall number of eight sensor positions were located at radius $r/R = 0.87$ at different angles ϕ according to the schematic view delineated in figure 1(*b*). Drawing a sequence of one-dimensional velocity profiles, recorded consecutively during a measuring time of 120 s, illustrates the spatiotemporal flow shown in figure 9 for the case of an ordinary bubble plume at a gas flow rate of $0.83\,\mathrm{cm^3\,s^{-1}}$. Here, the abscissa corresponds to the time line, whereas the measuring

depth of the particular velocity profiles being identical to the height Z/H is plotted along the ordinate. The colouring represents the amplitude of the vertical velocity. The principal situation becoming apparent in figure 9 has already been realized by analysing the time-averaged velocity data in § 3.2. In the case of the ordinary bubble plume without magnetic field a permanent downward flow can be observed in a zone from about 30 to 70 cm below the free surface. Occasionally, this zone is stretched towards the central part of the fluid cylinder, whereas in the bottom part a weak ascending motion can be observed. Apart from local velocity fluctuations the global flow pattern appears to be quasi-stationary. Figure 9(*b*) displays the velocity time series obtained at the position $Z/H = 0.5$ mm, also marked as black dashed, horizontal line in figure 9(*a*).

The imposition of a magnetic field leads to distinct modifications of the global flow structure. Figure 10 contains the corresponding spatiotemporal plots of the vertical velocity for Hartmann numbers of 162, 271 and 484. Drawing of the velocity profiles obtained in the perpendicular plane (figures 10(*a*), 10(*c*) and 10(*e*)) uncovers two separate regions with a predominantly descending flow. A spot with a strong negative, i.e. downwards directed, velocity is quasi-periodically moving from the free surface downwards. Reaching approximately the middle of the fluid container it returns abruptly to the location of departure. As shown in the picture, these downward flow domains are reciprocally paired with localized upward flow zones. This local inversion of the vertical velocity occurs only each second period for $Ha = 271$ and almost disappears at $Ha = 484$. The second descending flow region can be observed close to the bottom of the vessel. With increasing Hartmann number there is a tendency to establish a dominant recirculation zone showing maximum values of the downwards flow around the container mid-height. A similar pattern with an opposite sign of the velocity amplitude appear in the parallel plane at $\phi = 0$ as shown in figures 10(*b*), 10(*d*) and 10(*f*). The existence of dominating low-frequency flow structures is also reflected by the velocity time series in figure 11 obtained at $Z/H = 0.5$. The time period of the velocity signals recorded at $Ha = 162$ is about 30 s. Obviously, the time period as well as the amplitude of the low-frequency oscillations decline with increasing Hartmann number. The overall magnitude of the velocity in the parallel plane increases with growing magnetic field strength, whereas the temporary values oscillate between zero and a maximum value.

Measurements with variations of the gas flow rate were performed in the range $Q_g = 0.33$–$3.67\,\mathrm{cm^3\,s^{-1}}$. The outcome of these experiments showed that the phenomena observed are similar and the trends already described above can be generalized. As a second example we present results obtained at a gas flow rate of $Q_g = 3.67\,\mathrm{cm^3\,s^{-1}}$. Figures 12, 13 and 14 show the spatiotemporal structure, local velocity time series, as well as the corresponding frequency spectra, calculated using FFT, for the same set of Hartmann numbers as used in figures 10 and 11. Also at this gas flow rate distinct similarities can be noticed considering the spatiotemporal flow structures in both planes ($\phi = 0$ and $\phi = \pi/2$). Very regular oscillations have been found at $Ha = 162$ in the perpendicular plane (figure 12*a*). Zones with a high-intensity descending flow appear periodically beneath the free surface and move continuously towards the container bottom. The power spectra of the time series recorded at $Ha = 162$ in figures 13(*a*) and 14(*a*) reveal frequency peaks at 0.127 Hz and 0.131 Hz for the flow in the parallel and the perpendicular plane, respectively. Increasing the Hartmann number creates another flow pattern, as shown in figures 12(*c*) and 12(*d*). Regions with alternating ascending and descending fluid motion emerge. The FFT of the time series shows a distinct peak at 0.067 Hz for the time series in both planes. The large-scale

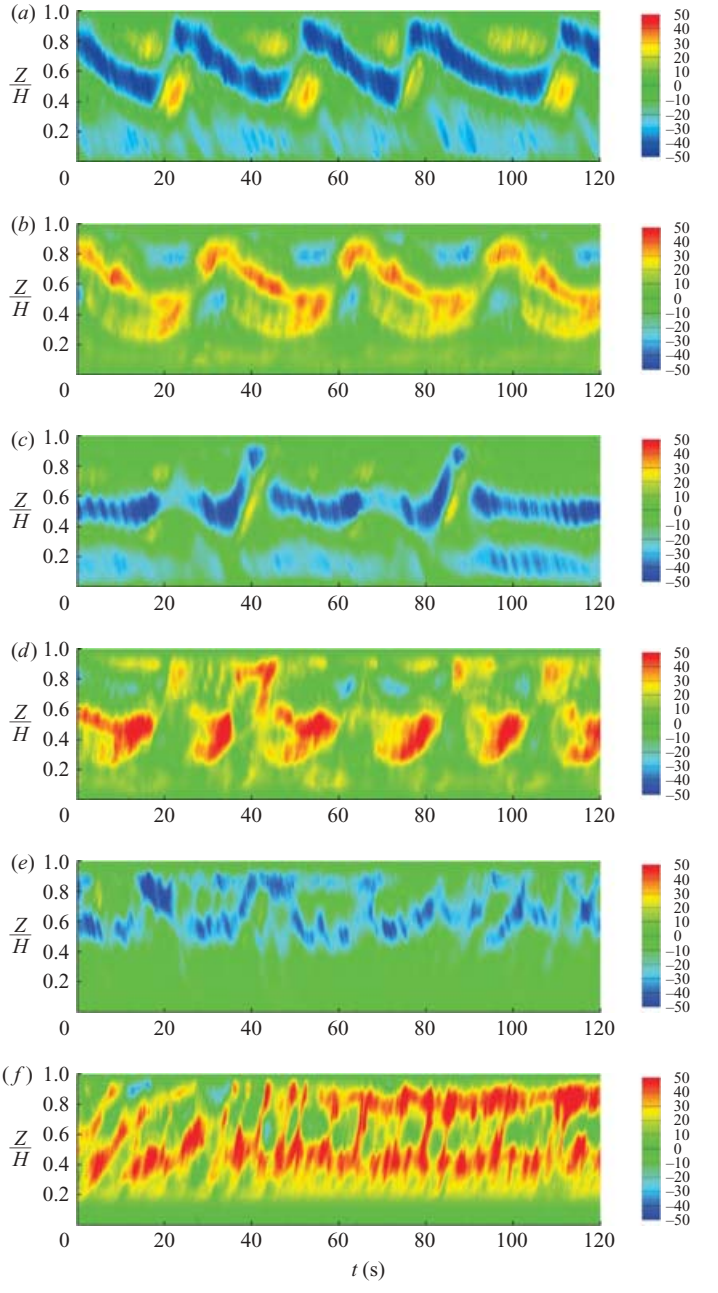

FIGURE 10. Spatiotemporal distributions of the vertical velocity component along a vertical line at various Hartmann numbers: (*a*), (*b*) $Ha = 162$; (*c*), (*d*) $Ha = 271$; (*e*), (*f*) $Ha = 484$. Figures (*a*), (*c*), (*e*) depict the flow in the perpendicular plane; and (*b*), (*d*), (*f*) depict the flow in the parallel plane. ($Q_g = 0.83\,\mathrm{cm^3\,s^{-1}}$.) The colour bar denotes the velocity in $\mathrm{mm\,s^{-1}}$.

fluctuations disappear almost completely if the Hartmann number reaches a value of 484. Here, stable zones of descending (perpendicular plane) or ascending (parallel plane) flows exist. Consequently, no dominant frequency peaks can be identified in the FFT spectra. Comparing the measurements, it is worth noting that the maximum

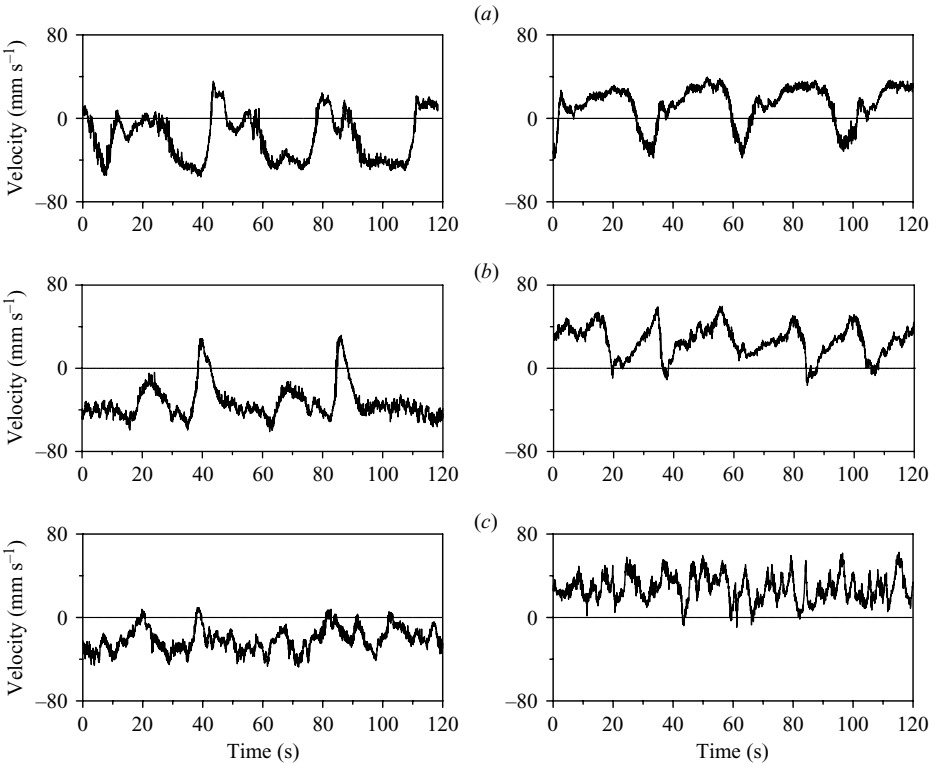

FIGURE 11. Time series of the vertical velocity component at different Hartmann numbers: (*a*) $Ha = 162$; (*b*) $Ha = 271$; (*c*) $Ha = 484$. Figures on the left present the flow in the perpendicular plane; on the right the flow in the parallel plane. The data were acquired at the position $r/R = 0.87$, $Z/H = 0.5$ applying a gas flow rate of $Q_g = 0.83\,\mathrm{cm^3\,s^{-1}}$.

amplitude of the velocity oscillations is found at $Ha = 271$. The time-averaged velocity even increases in the case of the highest magnetic field strength ($Ha = 484$), whereas the amplitude of the large-scale oscillations is substantially damped.

Values for the predominant frequencies determined from the power spectra of the velocity time series are plotted versus the gas flow rate in figure 15. The increase of the gas flow rate leads to higher frequencies in general. The significant enhancement registered at $Ha = 162$ for $Q_g > 3\,\mathrm{cm^3\,s^{-1}}$ is apparent.

Further measurements were carried out at a gas flow rate of $3.67\,\mathrm{cm^3\,s^{-1}}$ and a Hartmann number of 271 to obtain profiles of the vertical velocity simultaneously at different azimuthal locations ϕ at a radial coordinate of $r/R = 0.87$, whereas additional measuring positions located between the parallel and the perpendicular plane were also taken into consideration (see figure 1*b* for the arrangement). All the time series and the derived correlation functions presented here were obtained at a height of $Z/H = 0.77$. Auto-correlation and cross-correlation functions were calculated according to the following formulas:

$$R(\phi_1, \phi_1, \tau) = \frac{\overline{u(\phi_1, t) \cdot u(\phi_1, t + \tau)}}{\overline{u(\phi_1, t)^2}}, \tag{3.1}$$

$$R(\phi_1, \phi_2, \tau) = \frac{\overline{u(\phi_1, t) \cdot u(\phi_2, t + \tau)}}{\sqrt{\overline{u(\phi_1, t)^2} \cdot \overline{u(\phi_2, t)^2}}}. \tag{3.2}$$

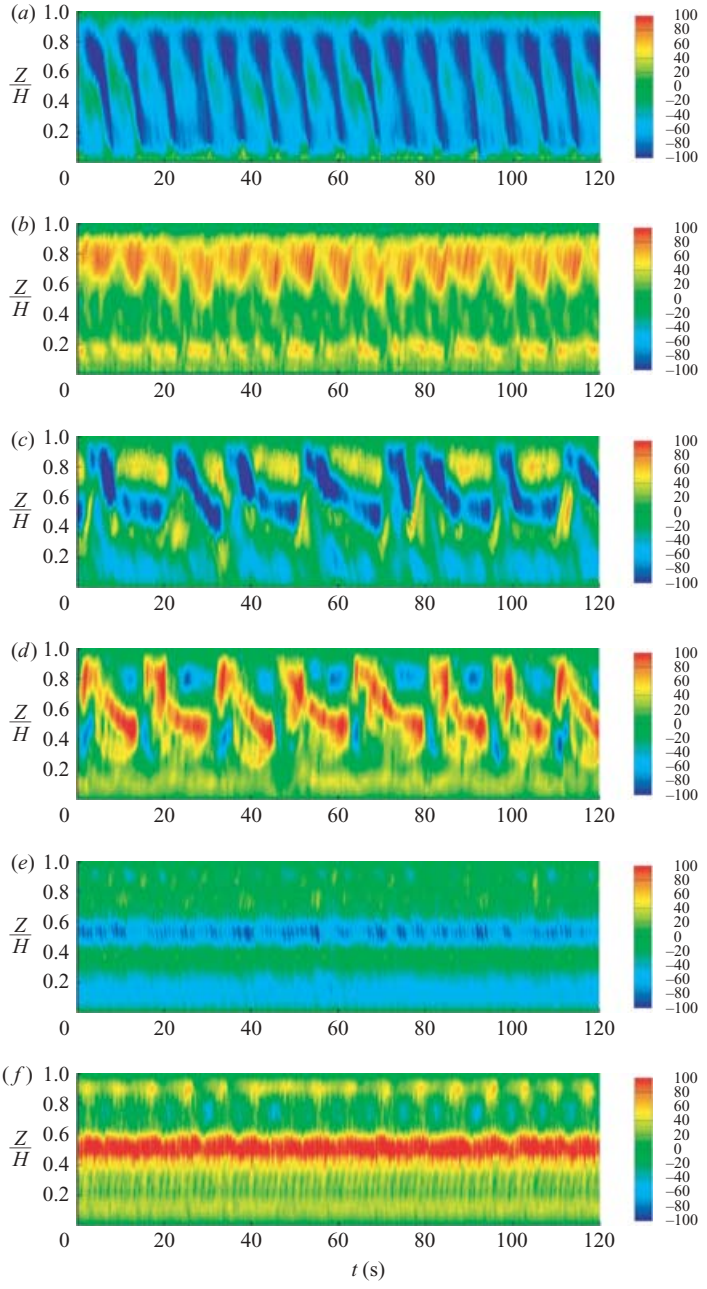

FIGURE 12. Spatiotemporal distributions of the vertical velocity along a vertical line at various Hartmann numbers: (*a*), (*b*) $Ha = 162$; (*c*), (*d*) $Ha = 271$; (*e*), (*f*) $Ha = 484$. Figures (*a*), (*c*), (*e*) depict the flow in the perpendicular plane; and (*b*), (*d*), (*f*) depict the flow in the parallel plane. ($Q_g = 3.67\,\mathrm{cm^3\,s^{-1}}$). The colour bar denotes the velocity in $\mathrm{mm\,s^{-1}}$.

Simultaneous measurements of the vertical velocity were performed at

(i) $\phi = 0$ and $\phi = \pi$,
(ii) $\phi = \pi/4$ and $\phi = 3\pi/4$,
(iii) $\phi = -\pi/4$ and $\phi = -3\pi/4$,
(iv) $\phi = 0$, $\phi = \pm\pi/4$ and $\phi = \pi/2$,

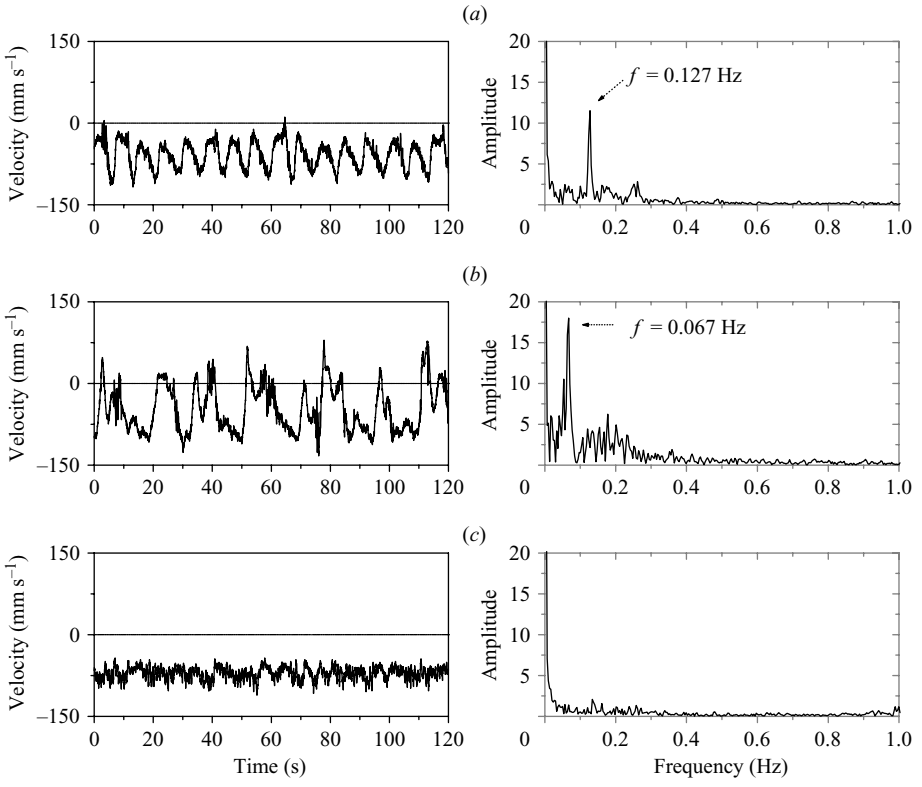

FIGURE 13. Velocity time series and corresponding FFT spectra of the vertical velocity component at different Hartmann numbers in the plane perpendicular to $\boldsymbol{B}$: (*a*) $Ha = 162$; (*b*) $Ha = 271$; (*c*) $Ha = 484$. The data were acquired at the position $r/R = 0.87$, $Z/H = 0.5$ applying a gas flow rate of $Q_g = 3.67\,\mathrm{cm^3\,s^{-1}}$.

allowing us to examine the relation of the velocity time series along chordal lines parallel and across the magnetic field direction, respectively. If the magnetic field provokes an elongation and alignment of the flow structures into the direction of the applied magnetic field (see Davidson 1995), a high degree of correlation should be found considering velocity signals obtained at chords aligned with the magnetic field lines. These results are expected to differ substantially from the correlation functions at $Ha = 0$ as depicted in first graph of figure 16. In fact, the comparison between autocorrelation functions calculated at $\phi = \pm\pi/4$ and cross-correlation functions $R(\pi/4, 3\pi/4)$ and $R(-\pi/4, -3\pi/4)$, respectively, demonstrates an almost perfect agreement. Regular oscillations occur showing a periodicity of about 16 s. The velocity time series obtained at $\phi = 0$ and $\phi = \pi$ were found to be highly correlated as well. At first sight it might be surprising that the degree of correlation along the diameter is less compared to the parallel chords. While the parallel chords are located outside the bubble plume, one has to take into consideration the occurrence of the rising bubbles at the midplane, which might disturb the spreading of momentum along the magnetic field lines and, therefore, be responsible for the weak distortion of the correlation function. Another evident feature is the appearance of another oscillating mode leading to a doubling of the frequency observable in the correlation functions $R(0, 0)$ and $R(0, \pi)$.

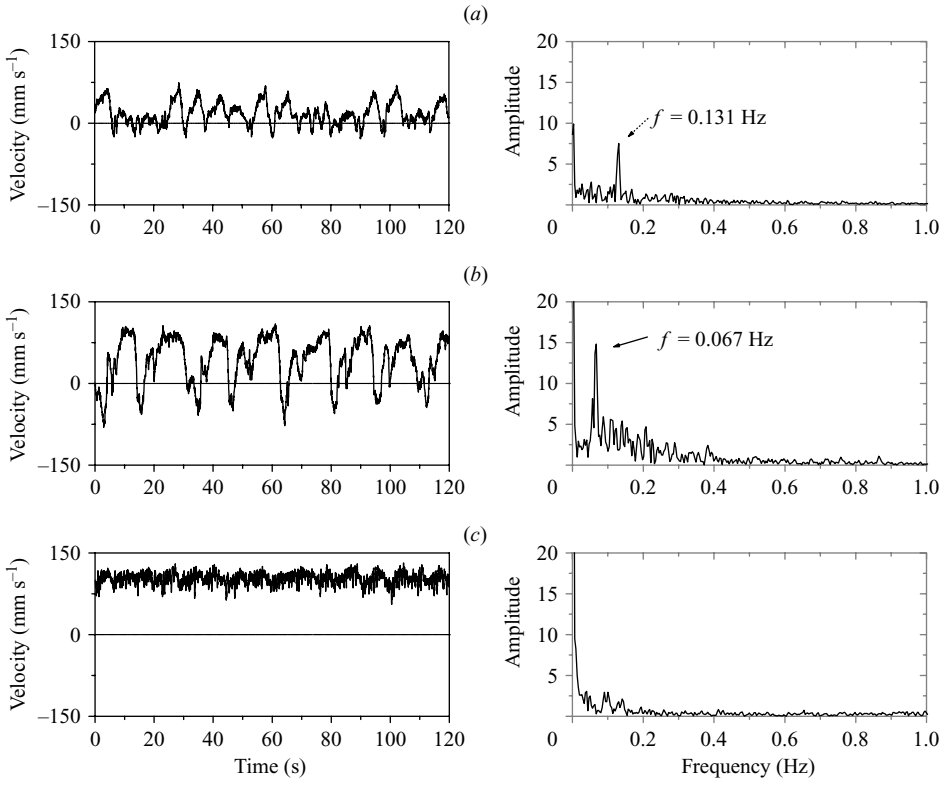

FIGURE 14. Velocity time series and corresponding FFT spectra of the vertical velocity component at different Hartmann numbers in the plane parallel to $\boldsymbol{B}$: (*a*) $Ha = 162$; (*b*) $Ha = 271$; (*c*) $Ha = 484$. The data were acquired at the position $r/R = 0.87$, $Z/H = 0.5$ applying a gas flow rate of $Q_g = 3.67\,\mathrm{cm^3\,s^{-1}}$.

This twofold frequency can also be recognized in figure 17 showing the time series of the vertical velocity component recorded in the parallel plane ($\phi = 0$), the perpendicular plane ($\phi = \pi/2$) and at the positions $\phi = \pm\pi/4$. Related auto-correlation and cross-correlation coefficients can be found in figure 18. All the four time series in figure 17 exhibit oscillations with a dominating periodicity around 16 s corresponding to a frequency of approximately 0.06 Hz, which is clearly confirmed by outstanding peaks in the spectra (not shown here). The velocity series at $\phi = \pi/2$ and $\phi = \pi/4$ show a positive concurrence, while on the other hand the time series obtained at $\phi = \pm\pi/4$ are negatively correlated. Thus, in the case of the magnetic field application the fluid motion in each half-volume delimited by the midplane parallel to the magnetic field direction becomes uniform along the field lines. The half-volumes on both sides of the parallel midplane are filled out with anisotropic, large-scale vortical flow structures oriented parallel to the magnetic field lines. The position of these vortices, which are expanded between the midplane and the near-wall region, is changing in time. A further question remains with respect to the temporal relation between the vortical structures in the half-volumes on both sides of the parallel midplane. As shown in figure 18, velocity time series recorded at $\phi = \pi/4$ and $\phi = -\pi/4$ are found to be in antiphase, indicating a reciprocal succession of vortical structures at both positions characterized by a phase lag of about half a period. The amplitude of velocity variations observed at $\phi = 0$ is considerably smaller compared to those at the

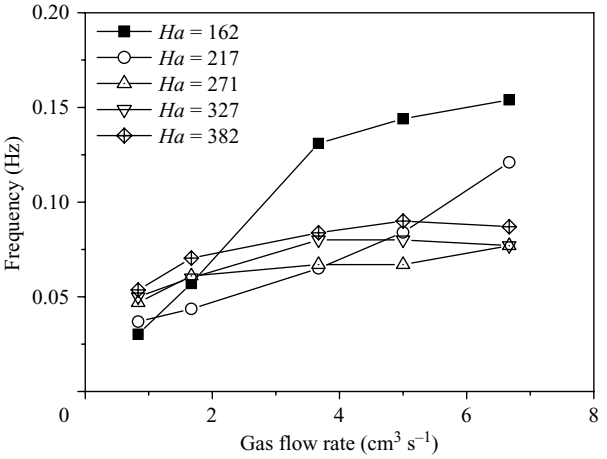

FIGURE 15. Predominant frequency of the vertical velocity at different gas flow rates and various Hartmann numbers. The measurements were performed in the perpendicular plane at $r/R = 0.87$, $Z/H = 0.5$.

other three measuring positions. Here, the flow is mainly ascending: the originally downward flow in the ordinary hydrodynamic situation has been reversed due to the electromagnetic force. In addition to the primary oscillation, another periodicity of about 8 s is manifested by smaller velocity peaks. The comparison between the time series in figure 17 shows that the peaks of ascending flow at $\phi = 0$ correspond at any one time to a maximum of descending flow at $\phi = \pm \pi/4$. This is understandable, because the interlaced progression of vortices occurring in both half-volumes with a periodicity of about 16 s should be registered at the midplane with a time shift of 8 s. However, it is worth noting that in our measurements along the entire height of the fluid vessel this twofold frequency could not be so clearly identified at all vertical positions. This is an indication that the flow symmetry with respect to the midplane parallel to the magnetic field is not perfect. Whilst, at several heights, the vortical structures occurring at both sides of the parallel midplane can be traced at $\phi = 0$, in other regions the velocity variations recorded at the parallel midplane are exclusively governed by the vortices from either of both half-volumes. Here, only a single peak of 0.06 Hz appears in the spectrum.

4. Discussion and concluding remarks

Davidson (1995) considered the generic problem of an initially axisymmetric jet, which is affected by a uniform magnetic field applied perpendicularly to the axis of motion. The imposed magnetic field gives rise to a damping of the motion by the induced Lorenz force. Looking along the magnetic field lines, regions of reverse flow appear on both left-hand and right-hand sides of the central jet. Otherwise, the induced electric current flowing mainly in the direction perpendicular to both the initial flow and the magnetic field is forced to return through regions outside the jet area. By this means previously stagnant fluid is accelerated, leading to an elongation of the jet cross-section parallel to the field lines. Davidson (1995) showed that in this way the global momentum of the motion is conserved by a transfer of energy along the magnetic field direction. These general features with respect to the reorganization of the flow pattern were also observed in our experiment.

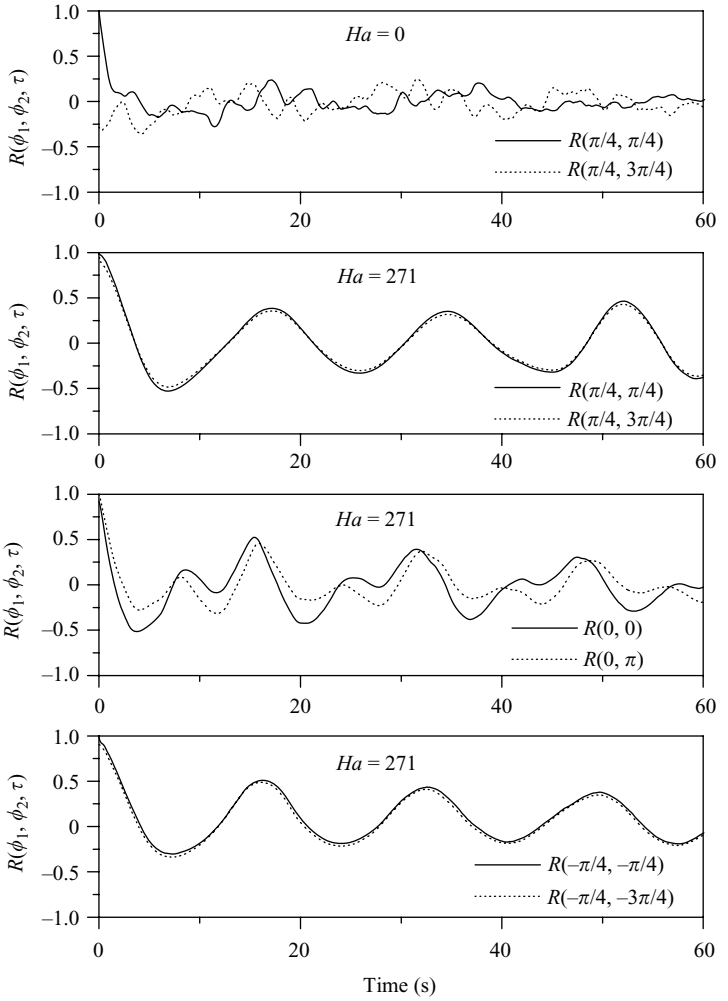

FIGURE 16. Correlation coefficients of the vertical velocity component along the direction of the magnetic field lines. (—— denotes the autocorrelation coefficient; ····· denotes the cross correlation coefficient.) All data were simultaneously measured at the position $r/R = 0.87$, $Z/H = 0.77$ applying a gas flow rate of $Q_g = 3.67\,\mathrm{cm^3\,s^{-1}}$.

For the case of a bubble-driven jet in a horizontal magnetic field, a promotion of ascending flow and suppression of the descending flow is visible in the plane parallel to the field lines while the situation was found to be vice versa in the plane perpendicular to the magnetic field. Owing to the application of a transverse magnetic field an axisymmetric, recirculating flow ceases to exist. Furthermore, the variation of the velocity parallel to the magnetic field decreases considerably. This is a clear indication of the development of quasi-two-dimensional flow structures already known from MHD turbulence (Sommeria & Moreau 1982). Already a weak magnetic field causes a suppression of three-dimensional perturbations. The kinetic energy thus released may partly be transferred to widespread vortices aligned with the magnetic field direction (Fauve *et al.* 1981). In fact, compared to the case $B = 0$ an increase of the RMS value of the vertical velocity has been found for moderate Hartmann numbers < 400. The ratio between the electromagnetic force and the inertial force

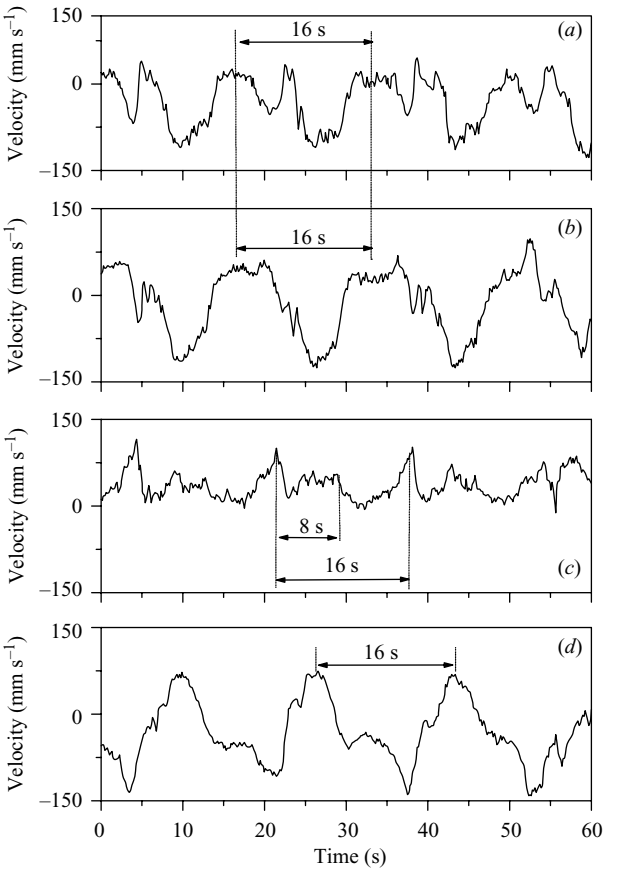

FIGURE 17. Time series of the vertical velocity component at different angular positions across the magnetic field lines: (*a*) $\phi = \pi/2$; (*b*) $\phi = \pi/4$; (*c*) $\phi = 0$; (*d*) $\phi = -\pi/2$. The velocities were simultaneously measured at the position $r/R = 0.87$, $Z/H = 0.77$ applying a Hartmann number of $Ha = 271$ and a gas flow rate $Q_g = 3.67\,\mathrm{cm^3\,s^{-1}}$.

can be estimated by calculating the interaction number N. For a gas flow rate of $Q_g = 3.67\,\mathrm{cm^3\,s^{-1}}$ in our experiment, a liquid velocity in the centre of the bubble plume of about $U_L \sim 200\,\mathrm{mm\,s^{-1}}$ has been found. Taking the container radius as the typical length scale, we obtain a Reynolds number of $Re \sim 2.4 \times 10^4$. Thus, for a Hartmann number $Ha = 162$, the magnetic interaction parameter is $N \sim 1$, and at the highest Hartmann number $Ha = 484$, we yield $N \sim 10$. In this parameter range the transition from three-dimensional turbulence to quasi-two-dimensional velocity structures is expected. In the present experiment the circular cross-section of the fluid cylinder obstructs the formation of perfect two-dimensional vortex columns parallel to the field lines. Nevertheless, the fluid motion is found to be dominated by large-scale structures elongated along the magnetic field direction over the entire chord lengths of the circular cross-section. Measurements of the vertical velocity in both planes parallel and perpendicular to the field lines, respectively, reveal this fact with an eye-catching, negative correlation of the recorded profiles. As long as the Hartmann number remains moderate the vertical position of these vortices oscillates. In particular, even counter-rotating vortices occur. At higher Hartmann numbers and magnetic interaction parameters $N \gtrsim 10$ the location of these recirculating zones

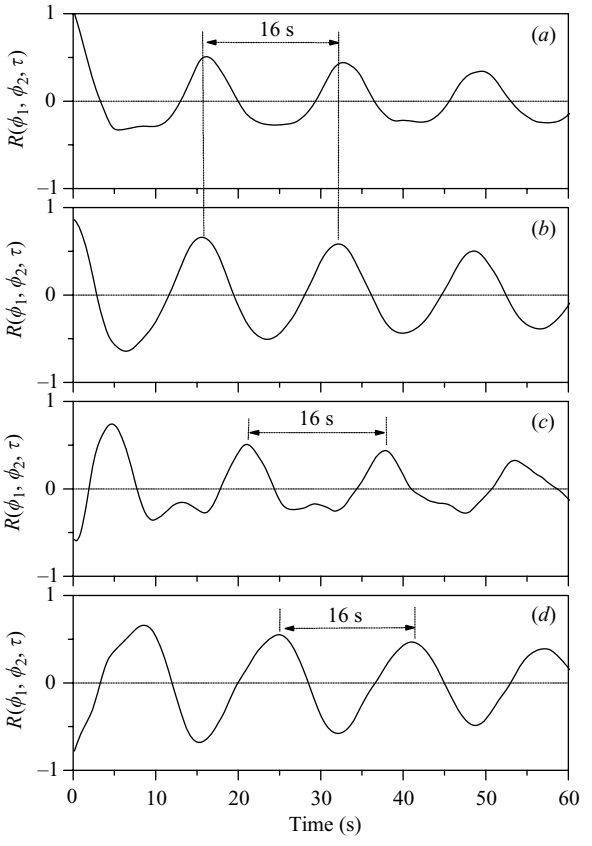

FIGURE 18. Correlation coefficients of the vertical velocity component corresponding to the velocity time series in figure 17: (*a*) autocorrelation coefficient $R(\pi/2, \pi/2)$ at $\phi = \pi/2$; (*b*) cross-correlation coefficient $R(\pi/4, \pi/2)$ at $\phi = \pi/4$; (*c*) cross-correlation coefficient $R(0, \pi/2)$ at $\phi = 0$; (*d*) cross-correlation coefficient $R(-\pi/4, \pi/2)$ at $\phi = -\pi/4$.

becomes frozen; however, it is not strictly accompanied by a lowering of the mean flow magnitude. A global damping of the flow was only observed at very small gas flow rate and the maximum magnetic field amplitude. Here, the magnetic interaction parameter N is assessed to be approximately 50.

An important issue is the appearance of strong flow oscillations due to the magnetic field application. Non-steady flow structures have been found which can be identified as travelling large-scale vortices. Owing to the direction of the applied magnetic field and the geometrical confinement, these vortices are allowed to move only in vertical direction, being similar to a propagation of waves. The separated progression of vortices in both half-volumes on either side of the cylinder midplane happens reciprocally. The formation and the transient behaviour of such large-scale flow structures reported in the present paper are supposed to explain the intensification of the convective heat transfer as observed in MHD thermal convection (Authie *et al.* 2003; Burr & Müller 2002; Burr *et al.* 2003) at moderate Hartmann numbers. At sufficiently high Hartmann numbers the vertical motion of the vortical structures will be suppressed, obviously associated with a reduction of the transfer properties. It becomes apparent that detailed measurements of the flow structure are also essential to fully understand the transport of scalar quantities, as for heat transfer phenomena.

Apart from the detailed characterization of the flow structures emerging in our experiment, the question concerning the mechanism responsible for a formation of the observed large-scale structures still remains difficult. The magnetic field primarily influences the liquid flow structure, but the driving force of the flow, i.e. the plume of the rising gas bubbles, is affected too. Therefore we cannot definitely conclude that the reinforced large-scale velocity fluctuations appearing in a particular range of Hartmann numbers represent a universal feature connected with the application of a DC magnetic field to any originally isotropic flow. For instance, it is known that the application of a transverse magnetic field increases the bubble drag coefficient (Eckert, Gerbeth & Lielausis 2000*b*) leading to an intensification of the momentum transfer between the gas and the liquid phase. At first sight such a deposition of a higher amount of kinetic energy in the liquid could be considered as another reason for the observed velocity oscillations. On the other hand, a strengthened acceleration of the liquid phase can also be realized by an increase of the gas flow rate. However, in our experiment it was not possible to initiate the travelling vortex structures at any gas flow rate as long as the magnetic field was zero. The aforementioned studies concerning the heat transfer in MHD flows (Authie *et al.* 2003; Burr & Müller 2002; Burr *et al.* 2003) suggest a similar behaviour of the flow. In contrast to an MHD flow in a straight channel at an ambient pressure drop, here we also have a free-developing flow; thus the considered phenomenon might well be typical for the application of a DC magnetic field on free convection. In the case of the bubble plume the flow is turbulent, showing velocity fluctuations on different length scales. It is well known that, due to the Joule dissipation, three-dimensional flow structures are quickly damped, whereas turbulent elements can survive if their vorticity is aligned with the magnetic field direction. Now it has been shown that under certain conditions these structures can also be amplified by a transfer of momentum leading to a reinforcement of velocity fluctuations, as observed in our experiment.

Local measurements of the bubble number using the conductance probes showed a periodic movement of the bubble plume along the container diameter perpendicular to the magnetic field, with a similar frequency as found to be typical for the detected velocity oscillations. This fact indicates a mutual interaction between the bubble plume and the travelling large-scale flow structures. The flow structures produce variations of the dynamic pressure, which are responsible for the wandering motion of the bubble plume in the two-phase system.

Such coupled oscillations between the lateral motion of the bubble plume and the velocity of the surrounding liquid have also been found in a conventional air-water system. Conventional bubble columns may exhibit a non-steady three-dimensional flow depending on various control parameters, like gas flow rate, aspect ratio or features of the gas injection system. Asymmetric flow pattern with distinct oscillations have been observed by Kuwagi & Ozoe (1999). The occurrence of an azimuthal flow at high void fractions up to 25 % was reported by Mudde, Groen & Van Den Akker (1997). The azimuthal component of the velocity was not measured in our experiments. We do not expect that a global azimuthal motion can exist in our experimental configuration, for the following reasons.

(i) The experiments were performed at low gas flow rates leading to maximum values of the void fraction up to 6 % at the cylinder axis at higher Hartmann numbers.

(ii) An azimuthal flow in the container would occur together with a helical motion of the bubble plume. Such a precession motion was not observed at the free surface (see also § 3.1).

(iii) An azimuthal flow is always connected with an axial component of vorticity. However, such flow structures are supposed to be effectively damped by a perpendicularly applied, horizontal magnetic field.

Becker, De Bie & Sweeney (1999) performed measurements in a cylindrical and a flat bubble column, respectively. The authors described the flow in the cylindrical vessel to be chaotic and not predictable. The velocity time series contain a broad range of low-frequency contributions, but there is no characteristic frequency for the entire column. A meandering bubble plume was observed in a flat rectangular bubble column. The velocity series in this case exhibit undamped harmonic oscillations connected to staggered rows of vortices moving downwards in a periodic way. The number of vortices increases with the liquid height: see Borchers *et al.* (1999). It is interesting to note that the application of a horizontal magnetic field on a bubble plume in a circular, liquid column as considered in our experiment leads to a flow structure similar to that known for flat bubble columns in ordinary hydrodynamics. In the latter case, the confinement of the container walls forced the flow to become two-dimensional, leaving mainly one horizontal vorticity component. In the MHD case the magnetic field causes the quasi-two-dimensional flow pattern. Moreover, the dominating frequency reported by Becker *et al.* (1999) is about 0.059 Hz, which is the same order of magnitude as found in our experiments. Naturally, the question arises whether the same mechanism is responsible for the occurrence of the velocity oscillations in both cases. Further work could more explicitly consider this similarity.

The feature that a static magnetic field may give rise to non-steady, non-isotropic large-scale flow structures could attain a key importance in metallurgical engineering, especially for the application of DC magnetic fields at the continuous casting process, where such an electromagnetic brake is suggested to stabilize the flow field. Note that the flow in such casting moulds is often a two-phase one because argon bubbles are injected into the melt to avoid clogging inside the casting nozzle. The potentially arising oscillations within a range of moderate field intensity need to be taken into account for future activities regarding further process optimization by means of an electromagnetic brake.

This investigation was conducted within the collaborative research centre SFB 609 'Electromagnetic Flow Control in Metallurgy, Crystal Growth and Electrochemistry'. The authors appreciate the financial support of this work by Deutsche Forschungsgemeinschaft (DFG).

REFERENCES

Authie, G., Tagawa, T. & Moreau, R. 2003 Buoyant flow in long vertical enclosures in the presence of a strong horizontal magnetic field. Part 2. Finite enclosures. *Eur. J. Mech.* B/*Fluids* **22**, 203–220.

Becker, S., De Bie, H. & Sweeney, J. 1999 Dynamic flow behaviour in bubble columns. *Chem. Engng Sci.* **54**, 4929–4935.

Borchers, O., Busch, C., Sokolichin, A. & Eigenberger, G. 1999 Applicability of the standard k-ϵ turbulence model to the dynamic simulation of bubble columns. Part II. Comparison of detailed experiments and flow simulations. *Chem. Engng Sci.* **54**, 5927–5935.

Brito, D., Nataf, H. C., Cardin, P., Aubert, J. & Masson, J. P. 2001 Ultrasonic Doppler velocimetry in liquid gallium. *Exps. Fluids* **31**, 653–663.

Burr, U. & Müller, U. 2001 Rayleigh–Bénard convection in liquid metal layers under the influence of a vertical magnetic field. *Phys. Fluids* **13**, 3247–3257.

Burr, U. & Müller, U. 2002 Rayleigh–Bénard convection in liquid metal layers under the influence of a horizontal magnetic field. *J. Fluid Mech.* **453**, 345–369.

Burr, U., Barleon, P., Jochmann, P. & Tsinober, A. 2003 Magnetohydrodynamic convection in a vertical slot with horizontal magnetic field. *J. Fluid Mech.* **475**, 21–40.

Cramer, A., Zhang, C. & Eckert, S. 2004 Local structures in liquid metals measured by ultrasonic Doppler velocimetry. *Flow Meas. Instrum.* **15**, 145–153.

Davidson, P. A. 1995 Magnetic damping of jets and vortices. *J. Fluid Mech.* **299**, 153–186.

Davidson, P. A. 2001 *An Introduction to Magnetohydrodynamics*. Cambridge University Press.

Eckert, S. & Gerbeth, G. 2002 Velocity measurements in liquid sodium by means of ultrasound Doppler velocimetry. *Exps. Fluids* **32**, 542–546.

Eckert, S., Gerbeth, G. & Lielausis, O. 2000*a* The behavior of gas bubbles in a turbulent liquid metal magnetohydrodynamic flow. Part I. Dispersion in quasi-two-dimensional magnetohydrodynamic turbulence. *Intl J. Multiphase Flow* **26**, 45–66.

Eckert, S., Gerbeth, G. & Lielausis, O. 2000*b* The behavior of gas bubbles in a turbulent liquid metal magnetohydrodynamic flow. Part II. Magnetic field influence on the slip ratio. *Intl J. Multiphase Flow* **26**, 67–82.

Fauve, S., Laroche, C., Libchaber, A. & Perrin, B. 1984 Chaotic phases and magnetic order in convective fluid. *Phys. Rev. Lett.* **52**, 1774–177111-122.7.

Iguchi, M., Demoto, Y., Sugawara, N. & Morita, Z. 1992 Bubble behavior in Hg-air vertical bubbling jets in a cylindrical vessel. *ISIJ Intl* **32**, 998–1005.

Iguchi, M.,Tsuji, Y., Mizuno, T., Mashiko, T., Sano, M. Kawabata, H., Ito, Y., NakaJima, K. & Morita, Z. 1994 Continuous measurements of bubble characteristics in a molten iron bath with Ar gas injection. *ISIJ Intl* **34**, 980–985.

Kuwagi, K. & Ozoe, H. 1999 Three-dimensional oscillation of bubbly flow in a vertical cylinder. *Intl J. Multiphase Flow* **25**, 175–182.

Leitch, A. M. & Baines, W. D. 1989 Liquid volume flux in a weak bubble plume. *J. Fluid Mech.* **205**, 77–98.

Milgram, J. H. 1983 Mean flow in round bubble plumes. *J. Fluid Mech.* **133**, 345–376.

Mudde, R. F. 2005 Gravity-driven bubbly flows. *Annu. Rev. Fluid. Mech.* **27**, 393–423.

Mudde, R. F., Groen, J. S. & Van Den Akker, H. E. A. 1997 Liquid velocity field in a bubble column: LDA experiments. *Chem. Engng Sci.* **52**, 4217–4224.

Papailiou, D. & Lykoudis, P. 1968 Magneto-fluid mechanic laminar natural convection: An experiment. *Intl J. Heat Mass Transfer* **11**, 1385–1391.

Serizawa, A., Kataoka, I. & Michiyshi, I. 1975 Turbulence structure of air–water bubbly flow. Part I. Measuring techniques. *Intl J. Multiphase Flow* **2**, 221–233.

Sommeria, J. & Moreau, R. 1982 Why, how, and when, MHD turbulence becomes two-dimensional. *J. Fluid Mech.* **118**, 507–518.

Tagawa, T. & Ozoe, H. 1997 Enhancement of heat transfer rate by application of a static magnetic field during natural convection of liquid metal in a cube. *J. Heat Transfer* **119**, 265–271.

Tagawa, T. & Ozoe, H. 1998 Enhanced heat transfer rate measured for natural convection in liquid gallium in a cubical enclosure under a static magnetic field, *J. Heat Transfer* **120**, 1027–1032.

Tagawa, T., Authie, G. & Moreau, R. 2002 Buoyant flow in long vertical enclosures in the presence of a strong horizontal magnetic field. Part 1. Fully-established flow. *Eur. J. Mech. B/Fluids* **21**, 383–398.

Takeda, Y. 1991 Development of an ultrasound velocity profile monitor. *Nucl. Engng Design* **126**, 277–284.

Takeda, Y. & Kikura, H. 2002 Flow mapping of the mercury flow. *Exps. Fluids* **32**, 161–169.

Tokuhiro, A. T. & Lykoudis, P. S. 1994 Natural convection heat transfer from a vertical plate. Part II. With gas injection and transverse magnetic field. *Intl J. Heat Mass Transfer* **37**, 1005–1012.

Wang, T., Wang, J., Ren, F. & Jin, Y. 2003 Application of Doppler ultrasound velocimetry in multiphase flow. *Chem. Engng J.* **92**, 111–122.

Zhang, C., Eckert, S. & Gerbeth, G. 2004 Gas and liquid velocity measurements in bubble chain driven two-phase flow by means of UDV and LDA. In *Proc. 5th Intl Conf. Multiphase Flow, Yokohama*, ICMF04-260.

Zhang, C., Eckert, S. & Gerbeth, G. 2005 Experimental study of single bubble motion in a liquid metal column exposed to a DC magnetic field. *Intl J. Multiphase Flow* **31**, 824–842.